rh-IFN-α Attenuates Neuroinflammation and Improves Neurological Function by Inhibiting NF-κB through JAK1-STAT1/TRAF3 Pathway in an Experimental GMH Rat Model

Peng Li[a,b,c,†], **Gang Zhao**[a,d,e,†], **Yan Ding**[a], **Tianyi Wang**[a], **Jerry Flores**[a], **Umut Ocak**[a], **Pei Wu**[a], **Tongyu Zhang**[a], **Jun Mo**[a], **John H. Zhang**[a,f], and **Jiping Tang**[a,*]

[a]Department of Physiology and Pharmacology, Basic Science, School of Medicine, Loma Linda University, Loma Linda, CA 92354

[b]Guangzhou First People's Hospital, Guangzhou Medical University, Guangzhou, China 510180

[c]Guangzhou First People's Hospital, the Second Affiliated Hospital of South China University of Technology, Guangzhou, China 510180

[d]Department of Emergency Surgery, the Second Affiliated Hospital of Kunming Medical University, Kunming, China 650101

[e]Traumatic Research Center of Yunnan Province, Kunming, China 650101

[f]Departments of Anesthesiology, Neurosurgery and Neurology, Loma Linda University School of Medicine, Loma Linda, CA 92354

Abstract

Neuroinflammation occurs after germinal matrix hemorrhage (GMH) and induces secondary brain injury. Interferon-α (IFN-α) has been shown to exert antiinflammatory effects in infectious diseases via activating IFNAR and its downstream signaling. We aimed to investigate the anti-inflammatory effects of Recombinant human IFN-α (rh-IFN-α) and the underlying mechanisms in a rat GMH model. Two hundred and eighteen P7 rat pups of both sexes were subjected to GMH by an intraparenchymal injection of bacterial collagenase. rh-IFN-α was administered intraperitoneally. Small interfering RNA (siRNA) of IFNAR, and siRNA of tumor necrosis factor receptor associated factor 3 (TRAF3) were administered through intracerebroventricular (i.c.v.) injections. JAK1 inhibitor ruxolitinib was given by oral lavage. Post-GMH evaluation included neurobehavioral function, Nissl staining, Western blot analysis, and immunofluorescence. Our results showed that endogenous IFN-α and phosphorylated IFNAR levels were increased after GMH. Administration of rh-IFN-α improved neurological functions, attenuated neuroinflammation, inhibited microglial activation, and ameliorated post-hemorrhagic

---

hydrocephalus after GMH. These observations were concomitant with IFNAR activation, increased expression of phosphorylated JAK1, phosphorylated STAT1 and TRAF3, and decreased levels of phosphorylated NF-κB, IL-6 and TNF-α. Specifically, knockdown of IFNAR, JAK1 and TRAF3 abolished the protective effects of rh-IFN-α. In conclusion, our findings demonstrated that rh-IFN-α treatment attenuated neuroinflammation, neurological deficits and hydrocephalus formation through inhibiting microglial activation after GMH, which might be mediated by IFNAR/JAK1-STAT1/TRAF3/NF-κB signaling pathway. Rh-IFN-α may be a promising therapeutic agent to attenuate brain injury via its anti-inflammatory effect.

Keywords

interferon-α; inflammation; germinal matrix hemorrhage; hydrocephalus; microglia

1. Introduction

Germinal matrix hemorrhage (GMH) is a devastating neonatal stroke, of which the complications include neuroinflammation, hydrocephalus, primary and secondary brain injury and developmental delay (Koschnitzky et al., 2018). Among all of the complications, the activation of inflammatory cascades could be the main contributing factor of a series of post-hemorrhagic consequences, such as long term morphological and functional impairment (Zhang et al., 2018; Feng Z et al., 2017). Therefore, inhibition of inflammatory response is critically important at the early stage after GMH. Microglia are resident immune cells in the central nervous system (CNS) (Tang J et al., 2017). Following GMH, microglia are activated immediately and release proinflammatory cytokines, such as tumor necrosis factor-α (TNF-α) and interleukin-6 (IL-6), leading to secondary brain injury (Brouwer et al., 2016). Thus, treatments focused on reducing proinflammatory cytokines by inhibiting microglia could be potentially important in attenuating neuroinflammation after GMH.

Interferon-α (IFN-α), one of type one interferons, can access the CNS to modulate microglial function in innate immune response (Owens et al., 2014). Binding to its receptor, IFN-α receptor (IFNAR), can activate the receptor-associated protein tyrosine kinases Janus kinases 1 (JAK1), which phosphorylates the latent cytoplasmic transcription factor signal transducer and activator of transcription 1 (STAT1). Currently, a number of studies have reported several pathways that link IFN-α with IFN-regulatory factors (IRF), toll-like receptors (TLRs), phosphatidylinositol 3 kinase (PI3K) and mitogen-activated protein kinases (MAPK) (L. Wang et al., 2010). On the other hand, the tumor necrosis factor receptor associated factor 3 (TRAF3) molecules are largely involved in signaling by a variety of adaptive and innate immune responses. TRAF3 signaling pathways typically lead to the activation of nuclear factor-κB (NF-κB) and IRFs, which is also related to immunomodulation (Tang et al., 2018). Although both IFN-α and TRAF3 were reported to interact with IRFs after inflammatory activation, it is still unknown whether TRAF3 is a downstream mediator of IFN-α in exerting its anti-inflammatory effect.

Therefore, based on the above mentioned evidence, we hypothesized that rh-IFN-α treatment would attenuate neuroinflammation after GMH by suppressing microglial

activation and consequently reduce the secretion of proinflammotory cytokines, improve neurological function in the short and long term and ameliorate posthemorrhagic hydrocephalus, and that these beneficial effects may be mediated by JAK1-STAT1/TRAF3/NF-κB signaling (Figure 1).

2. Materials and Methods

2.1. Animals

All experimental procedures were approved by the Institutional Animal Care and Use Committee at Loma Linda University. All studies were conducted in accordance with the United States Public Health Service's Policy on Humane Care and Use of Laboratory Animals and reported according to the ARRIVE guidelines. Two hundred and eighteen P7 Sprague-Dawley neonatal pups (weight=12-14g, Harlan, Livermore, CA) were randomly divided into Sham (n=36) and GMH (n=182) groups. All pups were housed with controlled temperature and 12-hour light/dark cycle, and given *ad libitum* access to food and water.

2.2 Experimental design

Seven separate experiments were performed in a rat model of GMH, as shown in Supplementary Figure 1. Total of two hundred and six pups were used as supplementary figure 5.

Experiment 1. The time course of endogenous IFN-α, its receptor IFNAR and phosphorylated IFNAR in the whole brain at 1, 3, 5, and 7 days after GMH was analyzed by Western blot. The cellular localization of IFNAR was detected by double immunofluorescence staining.

Experiment 2. The outcome of rh-IFN-α treatment was assessed during the first 3 days and 21-28 days after GMH. The pups were randomly divided into 5 groups: Sham, GMH+PBS, GMH+ rh-IFN-α (10^4U/kg), GMH+ rh-IFN-α (10^5U/kg), GMH+ rh-IFN-α (10^6U/kg). Exogenous rh-IFN-α (Millipore Sigma) was dissolved in phosphate-buffered saline (PBS) and administered in a total volume of 60μl intraperitoneally at 1 hour, 2 days and 3 days post-GMH. Short-term (negative geotaxis and body righting reflex) and long-term (rotarod test, foot fault and water maze) neurological tests were examined during the first 3 days and 21-28 days, respectively. Microglial activation was evaluated on the 3rd day after GMH by immunofluorescence staining.

Experiment 3. To identify the anti-neuroinflammatory effect of rh-IFN-α after GMH by blockage of endogenous IFN-β via intracerebroventricular injection of rat anti-IFN-β 24 hours prior to GMH induction and persistent intraperitoneal injection of anti-IFN-β once a day during the first 3 days after GMH. IL-6 and TNF-α levels were tested by Western blot on the 3rd day after GMH. Rats were divided into five groups: Sham, GMH + Vehicle, GMH + rh-IFN-α (10^5U/kg), GMH + rh-IFN-α (10^5U/kg) + anti-IFN-β isotype control, GMH + rh-IFN-α (10^5U/kg) + anti-IFN-β.

Experiment 4. To evaluate the effect of IFNAR *in vivo* on neuroinflammation after administration of rh-IFN-α post-GMH. IFNAR small interfering RNA (IFNAR siRNA) and

scramble siRNA (Scr siRNA) were infused via intracerebroventricular injection (i.c.v.) at 24 hours prior to GMH induction. The whole brain samples were collected to conduct Western blot testing on the 3rd day after GMH. The pups were randomly divided into five groups: Sham, GMH + Vehicle, GMH + rh-IFN-α (10^{5}U/kg), GMH + rh-IFN-α (10^{5}U/kg) + IFNAR siRNA, GMH + rh-IFN-α (10^{5}U/kg) + Scr siRNA.

Experiment 5. To access the role of JAK1-STAT1 pathway *in vivo* in neuroinflammation after administration of rh-IFN-α post-GMH. Ruxolitinib was administered via oral lavage at 24 hours prior to GMH induction and continued daily for three days. The whole brains were collected for Western blot on the 3rd day after GMH. The pups were divided randomly into Sham, GMH + Vehicle, GMH + rh-IFN-α (10^{5}U/kg), GMH + rh- IFN-α (10^{5}U/kg) + Ruxolitinib solvent, GMH + rh-IFN-α (10^{5}U/kg) + Ruxolitinib.

Experiment 6. To explore the role of TRAF3 in anti-neuroinflammation after administration of rh-IFN-α post-GMH. TRAF3 siRNA and Scr siRNA were administered via intracerebroventricular injection (i.c.v.) 24 hours prior to GMH induction. Brains were collected on the 3rd day after GMH. Rats were divided randomly into Sham, GMH + Vehicle, GMH+ re-IFN-α (10^{5}U/kg), GMH+re-IFN-α (10^{5}U/kg) +TRAF3 siRNA, GMH + re-IFN-α (10^{5}U/kg) + Scr siRNA.

Experiment 7. To evaluate the side effect of rh-IFN-α (10^{5}U/kg) administered during the first 3 days after GMH at 3 days and 28 days, respectively. The rats were divided randomly in two groups: naive and rh-IFN-α (10^{5}U/kg) treatment. Open field test and T maze were tested on the 28th day after treatment rh-IFN-α (10^{5}U/kg). The rat brains were collected on the 3rd day and 28th day after administration of rh-IFN-α (10^{5}U/kg) three times to analyze the expression of NeuN, GFAP and Synaptophysin.

2.3. Germinal matrix hemorrhage (GMH) model

The procedure for GMH model in unsexed P7 rats using collagenase infusion was performed as previously described (Feng et al., 2017). Briefly, pups were anesthetized with isoflurane (3.0% induction, 1-1.5% maintenance on a stereotaxic frame. After the skin was incised on the longitudinal plane and the Bregma was exposed, a 27-gauge needle with 0.3U clostridial collagenase (0.3 units of clostridial collagenase VII-S, Sigma-Aldrich, MO) was inserted (2.7 mm deep from the dura) through a burr hole drilled on the skull (1.6 mm lateral, 1.5 mm anterior to the Bregma) and infused (1 μl/min) using a 10 μl Hamilton syringe (Hamilton Co, Reno, NV, USA) guided by a microinfusion pump (Harvard Apparatus, Holliston, MA). The needle was kept in place for an extra 10 min to avoid leakage and withdrawn at speed of 0.5 mm/min. The pups were placed back to a heated blanket after infusion and euthanized at different time points according to the experimental design.

2.4. Drug administration

2.4.1. Recombinant human interferon-α—Recombinant human interferon-α (rh-IFN-α, Sigma-Adrich) was dissolved within phosphate-buffered saline (PBS) as described previously (Liu et al., 2016). Pups were administered different dosages (10^{4}U/kg, 10^{5}U/kg

and 10^6U/kg) or PBS via intraperitoneal injection at 1 hour post-GMH and then once daily for 3 days.

2.4.2.   *In vivo* RNA—Rat-derived IFNAR siRNA (0.5nm/2αl, Thermo Fisher), TRAF3 siRNA (0.5nm/2αl, Thermo Fisher) and Scramble siRNA (0.5nm/2αl, Thermo Fisher) were infused via intracerebroventricular injection (i.c.v.) at 24 hours prior to GMH induction (1.0mm anterior, 1.0 mm lateral to the Bregma and 1.7 mm deep on the contralateral hemisphere).

2.4.3.   Ruxolitinib—Ruxolitinib, dissolved in 2% dimethylsulfoxide, 30% polyethylene glycol (PEG) and dd H_2O, was administered via oral gavage with a lavage apparatus at 24 hours prior to GMH induction and persistently in the first 3 days after GMH(Heine et al., 2013; Shuey et al., 2016). Each rat was administered the dosage of 90mg/kg. Its solvent was administered as the vehicle control.

2.5.   Histological analysis

Pups were transcardially perfused under deep anesthesia with isoflurane (5%). Brains were removed and fixed in 10% formalin for 24 hours and then in 30% sucrose for 72 hour at 4 °C. Frozen coronal slices were sectioned as 10 μm for immunofluorescence (at 3 day after GMH) and 15 μm for Nissl staining (at 28 day after GMH) in a cryostat (CM3050S; Leica Microsystems, Wetzlar, Germany).

2.5.1.   Immunofluorescence—Double fluorescence staining was performed as described previously (Xie et al., 2017). Sections were blocked with 5% donkey serum for 1 hour and incubated at 4°C overnight with primary antibodies: rabbit anti-IFNAR (1:100, Antibodies online), mouse anti-NeuN (1:200, Abcam), chicken anti-GFAP (1:200, Abcam), and mouse anti-Iba1(1:100, Abcam) followed by incubation with appropriate fluorescence-conjugated secondary antibodies for 2 hours at room temperature. Negative control staining was performed by omitting the primary antibody. Fluorescence microscopy and LASX software were used to image the sections (Leica DMi8; Leica Microsystems, Wetzlar, Germany).

2.5.2.   Nissl staining—Nissl staining was conducted and analyzed as previously (Z. Wang et al., 2018). Brain sections were dehydrated in 95% and 70% ethanol for 2 min, and then washed in distilled water for 2 min. Sections were stained with 0.5% cresyl violet (Sigma-Aldrich, USA) for 2 min and washed in distilled water for 10s followed by dehydration with 100% ethanol and xylene for 2 min twice respectively before a coverslip with permount was placed. The volume of ventricular, gray matter loss, relative cortical thickness and relative white matter area were calculated with Image J 4.0 (Media Cybernetics). Calculations were performed in a blinded fashion.

2.6.   Western blot analysis

Brain tissues were collected and stored in −80°C freezer after being perfused with cold PBS (0.1M, pH 7.4) at 1d, 3d, 5d, and 7d for the time course study, at 3d for the mechanistic study after GMH induction separately, and at 3d and 28d after administration of IFN-α for

the side effect study. Western blot was processed as described previously (Nowsheen et al., 2018). After extraction of protein samples, protein quantification was performed using Lowry methodology (BioRad, USA). Each sample containing 50μg of protein were separated by SDS-PAGE gel electrophoresis, and then transferred onto nitrocellulose membrane. Membranes were blocked with milk and incubated with the following primary antibodies overnight at 4 °C: rabbit anti-interferon-α (Biomatik, USA), rabbit anti-IFNAR (antibodies-online, USA), rabbit anti-phospho-IFNAR (Thermofisher, USA), rabbit anti-JAK1(Abcam, USA), rabbit anti-phospho-JAK1(CST, USA),rabbit anti-STAT1(CST, USA), rabbit anti-phospho-STAT1 (CST, USA),mouse anti-TRAF3 (Abcam, USA), rabbit anti-NF-κB (Novusbio, USA), rabbit anti-phospho-NF-κB (CST, USA), rabbit anti IL-6 (Abcam, USA), rabbit anti TNF-α (Abcam, USA), goat anti-β-actin (Santa Cruz Biotechnology, USA), rabbit anti-NeuN (Abcam, USA), rabbit anti-GFAP (Abcam, USA), mouse anti-synaptophysin (Chemicon International, USA), and anti human interferon-α (Sigma, USA), β-actin was used as the internal loading control. Then, membranes were incubated with horseradish-peroxidase conjugated secondary antibodies (Santa Cruz Biotechnology, USA) for 1 h at room temperature. Membranes were probed with an ECL Plus chemiluminescence reagent kit (Amersham Biosciences, USA). The relative density of protein was analyzed by ImageJ software (ImageJ 1.5, NIH, USA).

2.7. Neurological tests

Neurological tests were performed blindly in a random and unbiased setup as previously reported (Segado-Arenas et al., 2017). Short-term neurological tests, as negative geotaxis and righting reflex, were conducted from 1d to 3d after GMH. Long-term neurological tests, including rotarod, foot fault and water maze were performed from 21-28d after GMH. Open field test and T maze were conducted 28d after administration of IFN-α for the side effect study.

2.7.1. Negative geotaxis—Negative geotaxis was tested to record the duration of the pups to turn 90° and 180° when positioned head downward on a 45° inclined plane. The maximum recording time was 60s (three trials/pup/day). The average value of all three trials were calculated.

2.7.2. Righting reflex—The pups were placed on the back onto a horizontal plane, and the time needed by the pup to right itself in a prone position on its four paws was recorded. The maximum recording time was 20s (three trials/pup/day). The average value of all three trials were calculated.

2.7.3. Rotarod test—The pups were placed on a rotating wheel (Columbus Instruments) and tested at a starting speed of 5-RMP and 10 RMP with acceleration at 2RPM per 5s. The time pups remained on the rotating wheel and the speed at which pups fell down from the rotarod were measured and averaged from 3 repeated trials.

2.7.4. Footfault—Foot-fault was recorded as the total numbers of missteps. When the pup's forelimb or hind limb fell into one of the grid openings, a foot fault was recorded. The maximum recording time was 60s.

2.7.5. Water maze test—According to our preliminary work and other similar studies, the water maze test was performed at 21-28 days after GMH. The water maze test used a circular pool (diameter: 110cm) filled with water at 24 ± 1 °C. A transparent escape platform (diameter: 11cm) was submerged 1 cm beneath the water and placed at a fixed position at the center of one of the quadrants. All pups underwent four trials per day with a 10 min inter-trial interval, for five consecutive days. In this process, pups needed to be guided to the platform if they did not find the platform. On Day 6, a probe trial was performed to assess spatial memory retention. During this trial, pups were allowed to swim freely for 60s, but no platform was present. Swim distance, latency, velocity and the percentage of time in targeting quadrant were digitally recorded and analyzed by a tracking software (Noldus Ethovision).

2.7.6. Open field test—A black rectangular box was used (100 cm × 100 cm × 45 cm) for the Open Field Test (OFT). The box was illuminated with three 30 W fluorescent bulbs placed 2 m above the box (Hou et al., 2018). The pups were placed in the corner of the box and allowed 10 min of exploration. The total distance travelled and the percent of time spent in the center were analyzed by a computerized video tracking system (Noldus Ethovision).

2.7.7. T-maze—Each pup was placed at the start area of the T-maze and allowed to choose an arm to enter. Once the pup selected an arm, it was confined to that arm for 30s and then returned to the start arm and confined there for 10s. Afterwards, the rat was allowed to choose an arm again. Ten trials were performed per pup. The total alternate numbers were recorded and repeated for 10 trials as corrected percentage for each animal.

2.8. Statistical analysis

All data were presented as a mean ± SD. All analyses were performed using GraphPad Prism 6 (GraphPad software). Data were first confirmed using the ShapiroWilk normality test. For the data that passed the normality test, the statistical differences among groups were further analyzed using one-way ANOVA followed by Tukey's multiple comparison *post hoc* analysis. For the data that failed the normality test, Kruskal-Wallis one-way ANOVA on Ranks was used, followed by Tukey's multiple comparison *post hoc* analysis. $P < 0.05$ was considered statistically significant.

3. Result

3.1. Endogenous IFN-α and phosphorylated IFNAR were upregulated after GMH.

Western blot results showed that there was a significant difference in the expression of endogenous IFN-α on the 3rd (df=25, P<0.001), 5th (df=25, P<0.001) and 7th (df=25, P<0.001) day after GMH (Fig. 2 A, B). The expression of phosphorylated IFNAR increased slowly from the 3rd day (df=25, p<0.001), peaked on the 5th day (df=25, p<0.001), and declined on the 7th day after GMH (p=0.003, Fig. 2 A, C). No changes were observed in the expression of IFNAR (Fig. 2A). Double immunofluorescence staining demonstrated that receptor IFNAR was abundantly expressed on neurons (Fig. 3A, B, C, and D), astrocytes (Fig. 3E, F, G, and H) and microglia (Fig. 3I, J, K, and L) on the 3rd day after GMH.

3.2. Intraperitoneal administration of human recombinant interferon-α improves short-term neurological function at 72h post GMH

Three dosages (10^4U/kg, 10^5U/kg and 10^6U/kg) of rh-IFN-α were performed via intraperitoneal injection 1h after GMH. Pups in the vehicle group took significantly more time to finish the action from head downward to the prone 90° (Fig. 4A) and 180° (Fig. 4B) position compared to the sham group in the first 3 days after GMH. There were significant differences in negative geotaxis between 3 treatment groups and vehicle on the 1st (df=29, 90°: *p<0.001, #p<0.001, &p<0.001; 180°: *p<0.001, #p<0.001, &p<0.001) and 2nd (df=29, 90°: *p<0.001, #p<0.001, &p<0.001; 180°: *p<0.001, #p<0.001, &p<0.001) day after GMH. Among these treatment groups, both the medium and high dosage of rh-IFN-α improved short-term neurological function in negative geotaxis and body righting reflex (df=29, *p<0.001, #p<0.001, Fig. 4C). Considering the safety of pups and the potential side effects, we chose the medium does of rh-IFN-α (10^5U/kg) for the following studies. Additionally, IFN-α was expressed in brain tissues on the third day after intraperitoneal injection post-GMH detected by Western blot (df=14, *p<0.001, #p<0.001, Fig. 4D, E), which confirmed that intraperitoneal administration of rh-IFN-α (10^5U/kg) was successfully delivered into the brain tissues.

3.3. rh-IFN-α treatment inhibited microglial response after GMH

In order to explore whether rh-IFN-α alters the microglial response after GMH, we used Iba-1 as microglial marker in the perihematoma area on the 3rd day after GMH. The result showed that the microglia in vehicle (Fig. 4I, J, and K) and treatment (Fig. 4L, M, and N) animals demonstrated bigger soma (Fig.4P) and shorter and more cell processes than sham animals (Fig. 4F, G, and H). The total number of microglia was decreased in rh-IFN-α treatment (df=17, #p=0.03, Fig. 4L, M, N and O) compared to Vehicle (Fig. 4I, J and K).

3.4. rh-IFN-α treatment ameliorated long-term neurological deficits post GMH

In the rotarod test, rh-IFN-α (10^5U/kg) treatment significantly decreased the falling speed and falling latency in both 5 rpm (df=33, # p<0.001, Fig. 5A, B) and 10 rpm (df=33, # p<0.001, Fig. 5A, B) acceleration compared to the vehicle group. In the foot fault test, pups in the vehicle group had significantly more total foot slips compared to the rh-IFN-α (10^5U/kg) treatment group (df=33, # p<0.001, Fig. 5C). Moreover, the water maze test showed that pups from the vehicle group swam significantly longer in 1 min (df=33, # p<0.001, Fig. 5E), took more time to find the platform (df=33, # p<0.001, Fig. 5F) and had less latency in the target quadrant during the probe trial (df=33, # p<0.001, Fig. 5G, H) compared to sham. In contrast, rh-IFN-α-treated pups performed better (df=33, # p<0.001, Fig. 5H) than vehicle. These findings indicated that rh-IFN-α treatment improved memory function at 28 days after GMH. There was no significant difference in swimming velocity among these 3 groups (df=33, p=0.089, Sham vs. GMH + Vehicle; p=0.969, Sham vs. GMH + rh-IFN-α; p=0.123, GMH + Vehicle vs. GMH + rh-IFN-α; Fig. 5D), meaning that the differences in finding the platform was related to the memory recovery, rather than the swimming ability. Studies have indicated that estrogen is a potent protective factor in young females in various stroke models (Ahnstedt et al., 2016; Faber et al., 2017). Thus, we categorized the behavioral data by sex to see if female pups were protected after GMH. Our

data showed that there was no difference between females (supplementary figure 2) and males (supplementary figure 3) in the long-term behavioral outcome after analyzing by sex.

3.5. rh-IFN-α treatment reduced ventricular dilation and gray matter loss, and increased cortical thickness and white matter area

Ventricular dilation is a major demonstration of PHH. We evaluated whether this could be attenuated by IFN-α treatment. Significant ventricular dilation (Fig. 6A) was observed in vehicle-treated pups, but the ventricular volume was reduced significantly by IFN-α treatment (df=14, *p<0.001; #p<0.001, Fig. 6B). Gray matter loss was significant in vehicle-treated animals, while it was also significantly attenuated with IFN-α treatment (df=14, *p<0.001, #p=0.0004, Fig. 6C). Loss of cortical tissues was significantly attenuated with IFN-α treatment (df=14,*p<0.001, #p<0.001, Fig. 6D) compared to vehicle-treated animals. Relative white matter area was significantly less in the vehicle group than that of sham and IFN-α treatment pups (df=14, *p<0.001, #p<0.001, Fig. 6E).

3.6. rh-IFN-α exerted anti-inflammatory effects after neutralizing endogenous interferon-β

Research has shown that during CNS inflammation, the production of endogenous IFN-I is locally up-regulated in the brain (Brendecke et al., 2012). In order to tease out the effect from endogenous IFN-β, we neutralized endogenous IFN-β with rat IFN-β antibody. The expression of inflammatory cytokines IL-6 (df=24, *p<0.001, #p<0.001, Fig. 7D, E) and TNF-α (df=24, *p<0.001, #p<0.001, Fig. 7D, F) was not significantly different from those treated by rh-IFN-α at 3 days after GMH. Moreover, there was no significant difference in the expression of inflammatory cytokines between IFN-β and isotype antibody group at 3 days after GMH. These data indicated that endogenous IFN-β did not interfere with the anti-inflammatory effect of IFN-α significantly after GMH.

3.7. Selective inhibition of IFNAR/JAK1-STAT1/TRAF3 pathways abolished the anti-inflammation of rh-IFN-α after GMH

3.7.1. Knockdown of IFNAR abolished the anti-neuroinflammation effects of rh-IFN-α post-GMH—Knockdown of IFNAR by specific siRNA significantly inhibited the expression of IFNAR and phosphorylated IFNAR in naive and GMH pups (df=19, *p<0.001, Sham vs. Sham + siRNA; *p<0.001, Sham vs. GMH + siRNA; #p<0.001, GMH vs. GMH + siRNA; Fig. 7A, B; Fig. 8; Fig. 9A2) at 3 days after intracerebraoventricular injection. Western blot results also showed that IFNAR siRNA significantly decreased phosphorylated JAK1 (df=30, &p<0.001, Scr siRNA vs. IFNAR siRNA, p=0.985>0.05, Sham vs. IFNAR siRNA, Fig. 8, Fig. 9A3), phosphorylated STAT1 (df=30, &p<0.001, Scr siRNA vs. IFNAR siRNA, p=0.978, Sham vs. IFNAR siRNA, Fig.8, Fig. 9A4) and TRAF3 (df=30, &p<0.001, Scr siRNA vs. IFNAR siRNA, p=0.978, Sham vs. IFNAR siRNA, Fig. 8, Fig. 9A5) expression, which was accompanied by increase of phosphorylated NF-κB (df=30, &p<0.001, Scr siRNA vs. IFNAR siRNA ; *p<0.001, Sham vs. IFNAR siRNA, Fig. 8, Fig. 9A6), IL-6 (df=30, &p<0.001, Scr siRNA vs. IFNAR siRNA; *p<0.001, Sham vs. IFNAR siRNA Fig. 8, Fig. 9A7) and TNF-α (df=30, &p<0.001, Scr siRNA vs. IFNAR siRNA ; *p<0.001, Sham vs. IFNAR siRNA Fig. 8, Fig. 9A8) at 3 days after GMH.

3.7.2. Inhibition of JAK1 reversed the anti-neuroinflammatory effect of rh-IFN-α after GMH

—Ruxolitinib was used as the inhibitor of JAK1. The results demonstrated that phosphorylated JAK1 (df=30, &p<0.001, Ruxolitinib Solvent vs. Ruxolitinib; p=0.1>0.05, Sham vs. Ruxolitinib, Fig. 8, Fig. 9B3) was declined significantly by ruxolitinib at 3 days after intraperitoneal injection, and the expression of phosphorylated STAT1 (df=30, &p<0.001, Ruxolitinib Solvent vs. Ruxolitinib; p=0.913>0.05, Sham vs. Ruxolitinib, Fig. 8, Fig. 9B4) and TRAF3 (df=30, &p<0.001, Ruxolitinib Solvent vs. Ruxolitinib; p=0.144, Sham vs. Ruxolitinib, Fig. 8, Fig. 9B5) decreased subsequently. However, phosphorylated NF-κB (df=30, &p<0.001, Ruxolitinib Solvent vs. Ruxolitinib; *p<0.001, Sham vs. Ruxolitinib, Fig. 8, Fig. 9B6), IL-6 (df=30, &p<0.001, Ruxolitinib Solvent vs. Ruxolitinib; *p<0.001, Sham vs. Ruxolitinib, Fig. 8, Fig. 9B7) and TNF-α (df=30, &p<0.001, Ruxolitinib Solvent vs. Ruxolitinib; *p<0.001, Sham vs. Ruxolitinib, Fig. 8, Fig. 9B8) elevated significantly at 3 days after GMH.

3.7.3. Decrease of the expression of TRAF3 exacerbated neuroinflammation after GMH

—The expression level of TRAF3 was significantly inhibited by its siRNA in naive and GMH pups 3 days after intracerebroventricular injection (df=19, *p<0.001, Sham vs. Sham + siRNA; *p<0.001, Sham vs. GMH + siRNA; #p<0.001, GMH vs. GMH + siRNA; Figure 6A and C; Figure 9C5). As shown in Fig.8C, inflammatory proteins, phosphorylated NF-κB (df=30, &p<0.001, Scr siRNA vs. TRAF3 siRNA; *p<0.001, Sham vs. TRAF3 siRNA, Fig. 8, Fig. 9C6), IL-6 (df=30, &p<0.001, Scr siRNA vs. TRAF3 siRNA; *p<0.001, Sham vs. TRAF3 siRNA, Fig. 8, Fig. 9C7) and TNF-α (df=30, &p<0.001, Scr siRNA vs. TRAF3 siRNA; *p<0.001, Sham vs. TRAF3 siRNA, Fig. 8, Fig. 9C8), were highly expressed after inhibition of TRAF3 3 days after GMH compared to the Scr siRNA group.

3.8. rh-IFN-α did not affect the expression of NeuN, GFAP, Synaptophysin and neurological behavior

Recently, some papers reported the side effects from IFN-α, such as psychiatric syndrome, after chronic administration. We analyzed the expression of NeuN, GFAP and synaptic related protein Synaptophysin in the cortex, striatum and hippocampus respectively at 3 days {Supplementary Figure 4A, B [df=9, p=0.196 (cortex), p=0.246 (striatum), p=0.068 (hippocampus)], C [df=9, p=0.586 (cortex), p=0.947 (striatum), p=0.506 (hippocampus)], D [df=9, p=0.483 (cortex), p=0.199 (striatum), p=0.675 (hippocampus)]} and 28 days (Supplementary Figure 4A, E [df=9, p=0.839 (cortex), p=0.778 (striatum), p=0.213 (hippocampus)], F [df=9, p=0.486 (cortex), p=0.746 (striatum), p=0.780 (hippocampus)], G [df=9, p=0.237 (cortex), p=0.277 (striatum), p=0.439 (hippocampus)]) after administration of rh-IFN-α. The result demonstrated that rh-IFN-α did not change the proportion of neurons, astrocytes and synaptic related protein Synaptophysin in these brain regions 3 days and 28 days after GMH. We also performed mood-related neurobehavioral tests 28 days after GMH. In an open field test, results showed no significance in total distance (df=9, p=0.996>0.05,Supplementary Figure 4H) and percentage of time in the center (df=9, p=0.323>0.05,Supplementary Figure 4I) between naive and rh-IFN-α treatment for 28 days. T-maze data revealed that the percentage of correct entries in rh-IFN-α treatment remained the same as naive group (df=9, p=0.1>0.05, Supplementary Figure 4 J).

4. Discussion

The incidence of GMH is approximately 50% in preterm infants between 24 and 30 weeks of gestation (Lekic et al., 2012; Koschnitzky et al., 2018). The newborn rat has neurodevelopmental similarities to preterm humans at 24-26 weeks. A previously publication also indicated that P7 Sprague-Dawley rats are comparable to 32 weeks of human gestational age. (Lekic T et al., 2015). GMH is a devastating neonatal stroke characterized as neuroinflammation, hydrocephalus, primary and secondary brain injury, neurodevelopmental delay (Agyemang et al., 2017). Furthermore, neuroinflammation is also a trigger of secondary injury after GMH. In our present study, we assessed the therapeutic effect of rh-IFN-α against neuroinflammation and explored the underlying mechanisms. Firstly, we observed the expression of endogenous IFN-α and phosphorylated IFNAR increased in the early phase after GMH, and receptor IFNAR was expressed on microglia, neurons and astrocytes. Additionally, administration of rh-IFN-α at the dosage of 10^5U/kg improved neurological functions and inhibited microglial activation in the first 3 days, and also attenuated the motor and memory dysfunction in long term. Moreover, knockdown of IFNAR using IFNAR siRNA exacerbated neuroinflammation, as shown by the decreased levels of phosphorylated IFNAR, phosphorylated JAK1, phosphorylated STAT1 and TRAF3 and increased in IL-6 and TNF-α. Furthermore, neuroinflammation also worsened after inhibiting JAK1 with ruxolitinib, concomitant with downregulation of phosphorylated JAK1, phosphorylated STAT1 and TRAF3, as indicated by the increased levels of IL-6 and TNF-α. The anti-neuroinflammatory effect was also abolished after silencing TRAF3 with TRAF3 siRNA, leading to upregulation of phosphorylated NF-κB, IL-6 and TNF-a. Finally, rh-IFN-α administrated on the 3rd day after GMH was tested in the brain but not in sham and vehicle, and also it did not change the expression of NeuN, GFAP and synaptophysin in cortex, striatum and hippocampus at 3 days and 28 days in the side effect study.

IFN-α belongs to the type one IFN family and is causally linked to the development of inflammatory encephalopathy (Murray et al., 2015; Sheehan et al., 2015). IFN-α has also been shown to limit production of inflammatory cytokines to prevent potential damage in neuroinflammation (Alammar L et al., 2011; Wang J et al., 2002). The brain injury is deteriorated by the activation of the inflammatory cascade, which is a major contributing factor in a series of other post-hemorrhagic complications (Dang et al., 2017). In this study, rh-IFN-α has been shown as an effective regulator involved in anti-neuroinflammation. We observed the expression of endogenous IFN-α and phosphorylated IFNAR were up-regulated as early as 3 days post-GMH, indicating a protective response to attenuate neuroinflammation. This data was consistent with previous research in encephalomyelitis (Ortego et al., 2014; Wei J et al., 2017). Our further studies showed that neurological deficits were attenuated significantly in short and long term after GMH. Hence, the improved neurological outcomes were attributed to neuroinflammatory inhibition by rh-IFN-α administration intraperitoneal injection which accessed the hemorrhagic brain.

The exact mechanism by which rh-IFN-α exerted its anti-neuroinflammatory effect in GMH still remains unclear so far. IFNAR(-/-) mice were more susceptible to infection and had more pronounced proinflammatory immune responses in various infectious models (Ortego et al., 2014). In our results, after knockdown of IFNAR by specific IFNAR siRNA, the result

that inflammatory cytokines IL-6 and TNF-α and classic phosphorylated NF-κB increased was consistent with viral infection outcome (Kothur K et al., 2016). Therefore, IFNAR could be an important target to attenuate inflammatory response after GMH.

Our current results revealed that the inflammation was deteriorated after inhibition of JAK1 and also led to the decrease of phosphorylated STAT1 on the 3rd day after GMH. Mounting research evidence has identified JAK-STAT axis as a major therapeutic target in suppressing various immune responses. IFNAR, as the receptor of IFN-α, is expressed on most cells, including microglia, and can activate and phosphorylate JAK1 and STAT1 after stimulation by pathological factors (Brendecke & Prinz, 2012; Murira et al., 2016). All of the above mentioned evidence supports our results observed in GMH.

It is known that TRAF3, belonging to the TRAF family, is an important immunomodulator, as it suppresses NF-κB p100 signaling (Yang et al., 2015). As shown in our results, after knockdown of IFNAR and JAK1 in GMH animals, TRAF3 expression was significantly reduced on the 3rd day, suggesting that TRAF3 might be a downstream factor of IFNAR and JAK1-STAT1 in the context of GMH. Meanwhile, decrease of TRAF3 promoted the expression of p-NF-κB and inflammatory cytokines IL-6 and TNF-α after inhibiting by specific siRNA on the 3rd day post GMH. In this process, after activation and phosphorylation of IFNAR by rh-IFN-α, an increase of TRAF3 mediated the degradation of NF-κB-inducing kinase (NIK) and served as a pivotal negative regulator of NF-κB p100 signaling (Yang & Sun, 2015; Yao et al., 2009; Tang X et al., 2018). Previous reports also showed that TRAF1 (Yu et al., 2018), TRAF2 (Schneider et al., 2012), and TRAF6 (Seijkens et al., 2018) mediated the anti-inflammatory effects in other disease models. Although we focused on TRAF3 on microglia in this study, we did not exclude the possibility that IFN-α activates other TRAF members and pathways in other cell types to inhibit inflammation, which will be our future research interest. According to what has been discussed above, our findings, coupled with the previous research, suggested that rh-IFN-α attenuated GMH-induced inflammation primarily mediated through the JAK1-STAT1/TRAF3/NF-κB pathway in microglia.

Some recent publications reported that the psychiatric syndrome, such as depression, was associated with administration of rh-IFN-α for 2 weeks (Dipasquale et al., 2016; Dowell et al., 2016). However, in our current study, the long-term behavior tests, namely open field test and T-maze, did not demonstrate a difference between naive and rh-IFN-α-treated animals on the 28th day. Furthermore, mature neuron marker NeuN, astrocyte marker GFAP and synaptic function related protein Synaptophysin did not change in the cortex, striatum and hippocampus on the 3rd day and 28th day between naive and rh-IFN-α-treated animals. This data suggested that short-phase treatment with rh-IFN-α did not elicit significant mood-related behavioral changes in animals nor did it alter the proportion of neurons and astrocytes.

There are some limitations in this current study. Besides the anti-neuroinflammatory effect of IFN-α, our study did not explore its potential neuroprotective effects on neurons in GMH. Additionally, *in vitro* study would eliminate the interplay between microglia and other cell types and further verify this signaling pathway that holds true in microglial reaction after

GMH. And in behavioral test for side effect, we need do more to reflect the depression, such as force swim, tail suspension or sucrose preference.

In conclusion, rh-IFN-α binding of IFNAR could attenuate neuroinflammation and improve neurological function through inhibiting NF-κB through the JAK1-STAT1/TRAF3 signaling pathway after GMH in a rat model. Therefore, rh-IFN-α may serve as a promising therapeutic agent against neuroinflammation and secondary brain injury for GMH patients.

Supplementary Material

Refer to Web version on PubMed Central for supplementary material.

Acknowledgments

Uncategorized References

Agyemang AA, Sveinsdottir K, Vallius S, et al. (2017). Cerebellar Exposure to Cell-Free Hemoglobin Following Preterm Intraventricular Hemorrhage: Causal in Cerebellar Damage? Transl Stroke Res. doi: 10.1007/s12975-017-0539-1

Ahnstedt H, McCullough LD, & Cipolla MJ (2016). The Importance of Considering Sex Differences in Translational Stroke Research. Transl Stroke Res, 7(4), 261–273. doi: 10.1007/s12975-016-0450-1 [PubMed: 26830778]

Alammar L, Gama L, Clements JE. Simian immunodeficiency virus infection in the brain and lung leads to differential type I IFN signaling during acute infection. J Immunol. 2011 4 1;186(7):4008–18. doi: 10.4049/jimmunol.1003757 [PubMed: 21368232]

Brendecke SM, & Prinz M. (2012). How type I interferons shape myeloid cell function in CNS autoimmunity. J Leukoc Biol, 92(3), 479–488. doi: 10.1189/jlb.0112043 [PubMed: 22661236]

Brouwer MJ, de Vries LS, Kersbergen KJ, et al. (2016). Effects of Posthemorrhagic Ventricular Dilatation in the Preterm Infant on Brain Volumes and White Matter Diffusion Variables at Term-Equivalent Age. J Pediatr, 168, 41–49 e41. doi: 10.1016/j.jpeds.2015.09.083 [PubMed: 26526364]

Dang G, Yang Y, Wu G, et al. (2017). Early Erythrolysis in the Hematoma After Experimental Intracerebral Hemorrhage. Transl Stroke Res, 8(2), 174–182. doi: 10.1007/s12975-016-0505-3 [PubMed: 27783383]

Dipasquale O, Cooper EA, Tibble J, et al. (2016). Interferon-alpha acutely impairs whole-brain functional connectivity network architecture - A preliminary study. Brain Behav Immun, 58, 31–39. doi: 10.1016/j.bbi.2015.12.011 [PubMed: 26697999]

Dowell NG, Cooper EA, Tibble J, et al. (2016). Acute Changes in Striatal Microstructure Predict the Development of Interferon-Alpha Induced Fatigue. Biol Psychiatry, 79(4), 320–328. doi: 10.1016/j.biopsych.2015.05.015 [PubMed: 26169252]

Faber JE, Moore SM, Lucitti JL, et al. (2017). Sex Differences in the Cerebral Collateral Circulation. Transl Stroke Res, 8(3), 273–283. doi: 10.1007/s12975-016-0508-0 [PubMed: 27844273]

Feng Z, Ye L, Klebe D, et al. (2017). Anti-inflammation conferred by stimulation of CD200R1 via Dok1 pathway in rat microglia after germinal matrix hemorrhage. J Cereb Blood Flow Metab, 271678X17725211. doi: 10.1177/0271678X17725211

Heine A, Held SA, Daecke SN, et al. (2013). The JAK-inhibitor ruxolitinib impairs dendritic cell function in vitro and in vivo. Blood, 122(7), 1192–1202. doi: 10.1182/blood-2013-03-484642 [PubMed: 23770777]

Hou L, Qi Y, Sun H, et al. (2018). Applying ketamine to alleviate the PTSD-like effects by regulating the HCN1-related BDNF. Prog Neuropsychopharmacol Biol Psychiatry. doi:10.1016/j.pnpbp. 2018.03.019

Koschnitzky JE, Keep RF, Limbrick DD Jr., et al. (2018). Opportunities in posthemorrhagic hydrocephalus research: outcomes of the Hydrocephalus Association Posthemorrhagic Hydrocephalus Workshop. Fluids Barriers CNS, 15(1), 11. doi: 10.1186/s12987-018-0096-3 [PubMed: 29587767]

Kothur K, Wienholt L, Mohammad SS, et al. Utility of CSF Cytokine/Chemokines as Markers of Active Intrathecal Inflammation: Comparison of Demyelinating, Anti-NMDAR and Enteroviral Encephalitis. PLoS One. 2016 8 30;11(8):e0161656. doi: 10.1371/journal.pone.0161656 [PubMed: 27575749]

Lekic T, Manaenko A, Rolland W, Krafft PR, et al. Rodent neonatal germinal matrix hemorrhage mimics the human brain injury, neurological consequences, and post-hemorrhagic hydrocephalus. Exp Neurol. 2012 7;236(1):69–78. doi: 10.1016/j.expneurol.2012.04.003 [PubMed: 22524990]

Lekic T, Klebe D, Poblete R, Krafft PR, et al. Neonatal brain hemorrhage (NBH) of prematurity: translational mechanisms of the vascular-neural network. Curr Med Chem. 2015;22(10):1214–38. [PubMed: 25620100]

Liu CC, Gao YJ, Luo H, et al. (2016). Interferon alpha inhibits spinal cord synaptic and nociceptive transmission via neuronal-glial interactions. Sci Rep, 6, 34356. doi: 10.1038/srep34356 [PubMed: 27670299]

Murira A, & Lamarre A (2016). Type-I Interferon Responses: From Friend to Foe in the Battle against Chronic Viral Infection. Front Immunol, 7, 609. doi: 10.3389/fimmu.2016.00609 [PubMed: 28066419]

Murray C, Griffin EW, O'Loughlin E, et al. (2015). Interdependent and independent roles of type I interferons and IL-6 in innate immune, neuroinflammatory and sickness behaviour responses to systemic poly I:C. Brain Behav Immun, 48, 274–286. doi: 10.1016/j.bbi.2015.04.009 [PubMed: 25900439]

Nowsheen S, Aziz K, Aziz A, et al. (2018). L3MBTL2 orchestrates ubiquitin signalling by dictating the sequential recruitment of RNF8 and RNF168 after DNA damage. Nat Cell Biol, 20(4), 455–464. doi: 10.1038/s41556-018-0071-x [PubMed: 29581593]

Ortego J, de la Poza F, & Marin-Lopez A (2014). Interferon alpha/beta receptor knockout mice as a model to study bluetongue virus infection. Virus Res, 182,35–42. doi:10.1016/j.virusres. 2013.09.038 [PubMed: 24100234]

Owens T, Khorooshi R, Wlodarczyk A, et al. (2014). Interferons in the central nervous system: A few instruments play many tunes. Glia, 62(3), 339–355. doi: 10.1002/glia.22608 [PubMed: 24588027]

Schneider M, Zimmermann AG, Roberts RA, et al. (2012). The innate immune sensor NLRC3 attenuates Toll-like receptor signaling via modification of the signaling adaptor TRAF6 and transcription factor NF-kappaB. Nat Immunol, 13(9), 823–831. doi: 10.1038/ni.2378 [PubMed: 22863753]

Segado-Arenas A, Infante-Garcia C, Benavente-Fernandez I, et al. (2017). Cognitive Impairment and Brain and Peripheral Alterations in a Murine Model of Intraventricular Hemorrhage in the Preterm Newborn. Mol Neurobiol. doi: 10.1007/s12035-017-0693-1

Seijkens TTP, van Tiel CM, Kusters PJH, et al. (2018). Targeting CD40-Induced TRAF6 Signaling in Macrophages Reduces Atherosclerosis. J Am Coll Cardiol, 71(5), 527–542. doi: 10.1016/j.jacc. 2017.11.055 [PubMed: 29406859]

Sheehan KC, Lazear HM, Diamond MS, et al. (2015). Selective Blockade of Interferon-alpha and -beta Reveals Their Non-Redundant Functions in a Mouse Model of West Nile Virus Infection. PLoS One, 10(5), e0128636. doi: 10.1371/journal.pone.0128636 [PubMed: 26010249]

Shuey DL, Oliver J, Zhou G, et al. (2016). Results from oral gavage carcinogenicity studies of ruxolitinib in Tg.rasH2 mice and Sprague-Dawley (Crl:CD) rats. Regul Toxicol Pharmacol, 81, 305–315. doi: 10.1016/j.yrtph.2016.09.016 [PubMed: 27647628]

Tang J, Miao H, Jiang B, et al. A selective CB2R agonist (JWH133) restores neuronal circuit after Germinal Matrix Hemorrhage in the preterm via CX3CR1+ microglia. Neuropharmacology. 2017 6; 119:157–169. doi: 10.1016/j.neuropharm.2017.01.027 [PubMed: 28153531]

Tang X, Zhang L, & Wei W (2018). Roles of TRAFs in NF-kappaB signaling pathways mediated by BAFF. Immunol Lett, 196, 113–118. doi: 10.1016/j.imlet.2018.01.010 [PubMed: 29378215]

Wang J, Schreiber RD, Campbell IL. STAT1 deficiency unexpectedly and markedly exacerbates the pathophysiological actions of IFN-alpha in the central nervous system. Proc Natl Acad Sci U S A. 2002 12 10;99(25):16209–14.doi: : 10.1073/pnas.252454799 [PubMed: 12461178]

Wang L, Gordon RA, Huynh L, et al. (2010). Indirect inhibition of Toll-like receptor and type I interferon responses by ITAM-coupled receptors and integrins. Immunity, 32(4), 518–530. doi: 10.1016/j.immuni.2010.03.014 [PubMed: 20362473]

Wang Z, Zhou F, Dou Y, et al. (2018). Melatonin Alleviates Intracerebral Hemorrhage-Induced Secondary Brain Injury in Rats via Suppressing Apoptosis, Inflammation, Oxidative Stress, DNA Damage, and Mitochondria Injury. Transl Stroke Res, 9(1), 74–91. doi: 10.1007/s12975-017-0559-x [PubMed: 28766251]

Wei J, Ma Y, Wang L, et al. Alpha/beta interferon receptor deficiency in mice significantly enhances susceptibility of the animals to pseudorabies virus infection. Vet Microbiol. 2017 5; 203:234–244. doi: 10.1016/j.vetmic.2017.03.022 [PubMed: 28619150]

Xie Z, Huang L, Enkhjargal B, et al. (2017). Recombinant Netrin-1 binding UNC5B receptor attenuates neuroinflammation and brain injury via PPARgamma/NFkappaB signaling pathway after subarachnoid hemorrhage in rats. Brain Behav Immun. doi: 10.1016/j.bbi.2017.11.012

Yang XD, & Sun SC (2015). Targeting signaling factors for degradation, an emerging mechanism for TRAF functions. Immunol Rev, 266(1), 56–71. doi: 10.1111/imr.12311 [PubMed: 26085207]

Yao Z, Xing L, & Boyce BF (2009). NF-kappaB p100 limits TNF-induced bone resorption in mice by a TRAF3-dependent mechanism. J Clin Invest, 119(10), 3024–3034. doi: 10.1172/JCI38716 [PubMed: 19770515]

Yu S, Wang M, Guo X, et al. (2018). Curcumin Attenuates Inflammation in a Severe Acute Pancreatitis Animal Model by Regulating TRAF1/ASK1 Signaling. Medical Science Monitor, 24, 2280–2286. doi: 10.12659/msm.909557 [PubMed: 29657313]

Zhang Y, Xu N, Ding Y, et al. (2018). Chemerin suppresses neuroinflammation and improves neurological recovery via CaMKK2/AMPK/Nrf2 pathway after germinal matrix hemorrhage in neonatal rats. Brain Behav Immun. doi: 10.1016/j.bbi.2018.02.015

Highlights

rh-IFN-α improves neurological behavior and attenuates post hemorrhagic hydrocephalus after GMH.

Rh-IFN-α inhibits neuroinflammation after GMH.

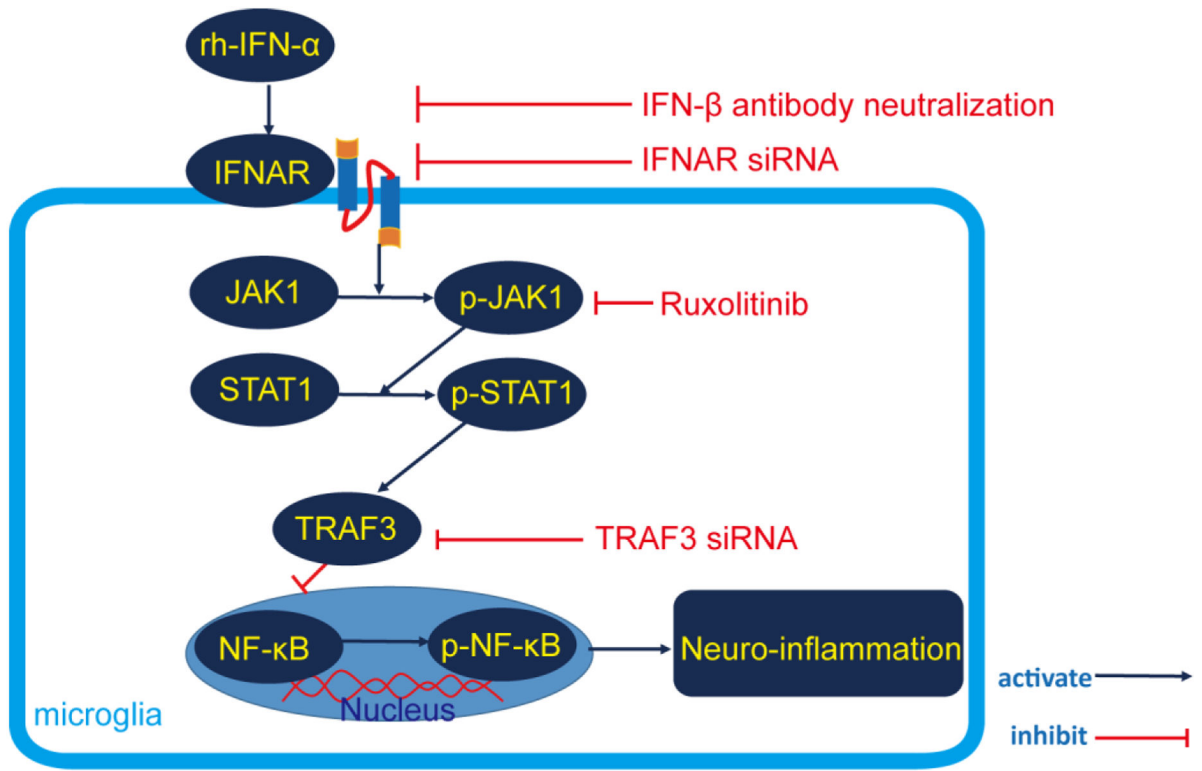Anti-inflammatory effect of Rh-IFN-α is mediated through IFNAR/JAK1-STAT1/ TRAF3/ NF-Kb pathway after GMH.
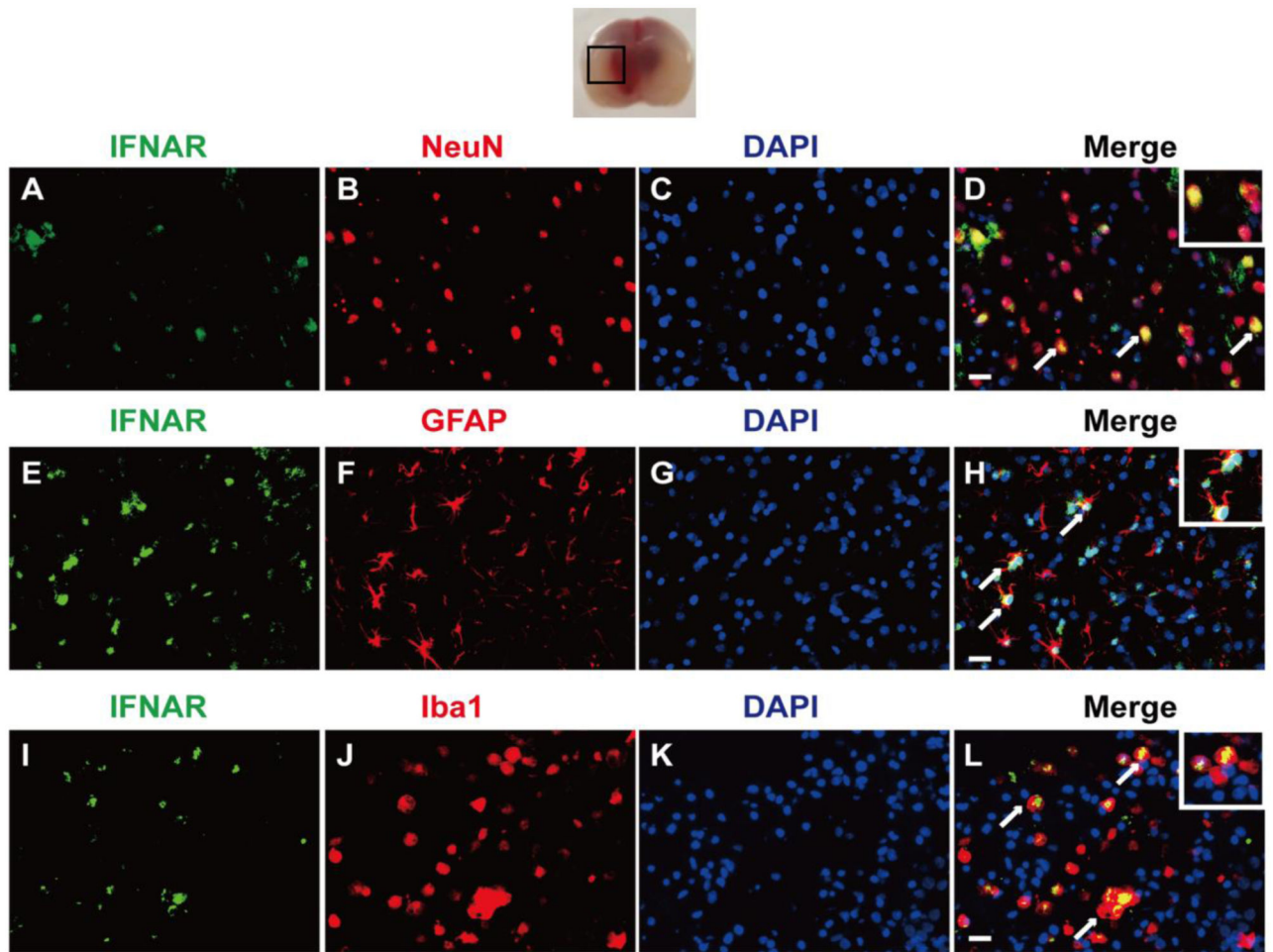
Figure 1.
Proposed pathway in this study.

Figure 2.
Time course of endogenous IFN-α, phosphorylated IFNAR (p-IFNAR) and IFNAR expression after GMH. Representative Western blot bands (A) and quantitative analysis of IFN-α (B), p-IFNAR and IFNAR (C) expression in the whole brains after GMH. Relative density of each protein has been normalized against the Sham group. n=6. *p<0.001 vs Sham.
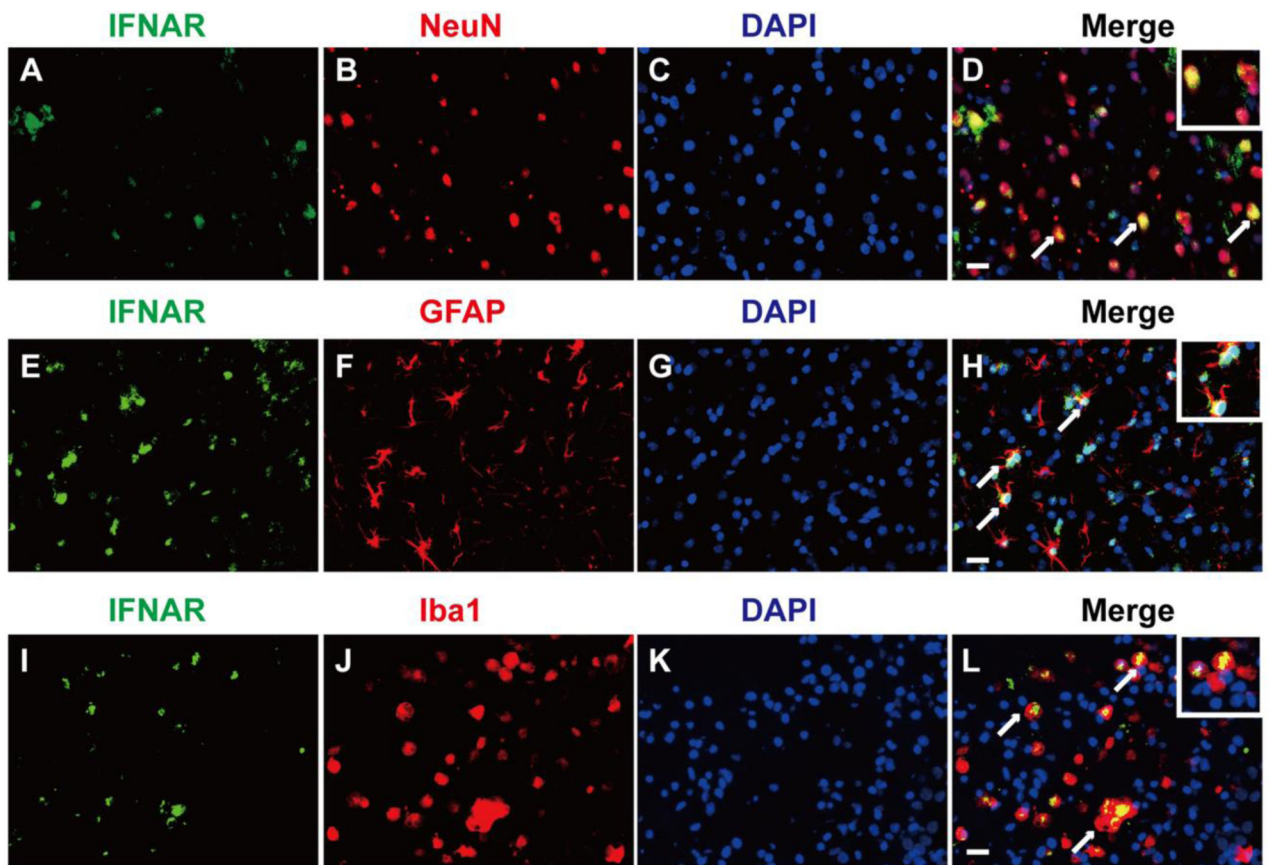
Figure 3.
The cellular localization of IFNAR in the perihematinoma area of brains. Representative of double immunofluorescence staining showed that IFNAR was expressed on neurons (A, B, C, and D), astrocytes (E, F, G, and H) and microglia (I, J, K, and L) on the 3rd day after GMH. n=2. Scale bar=50μm.
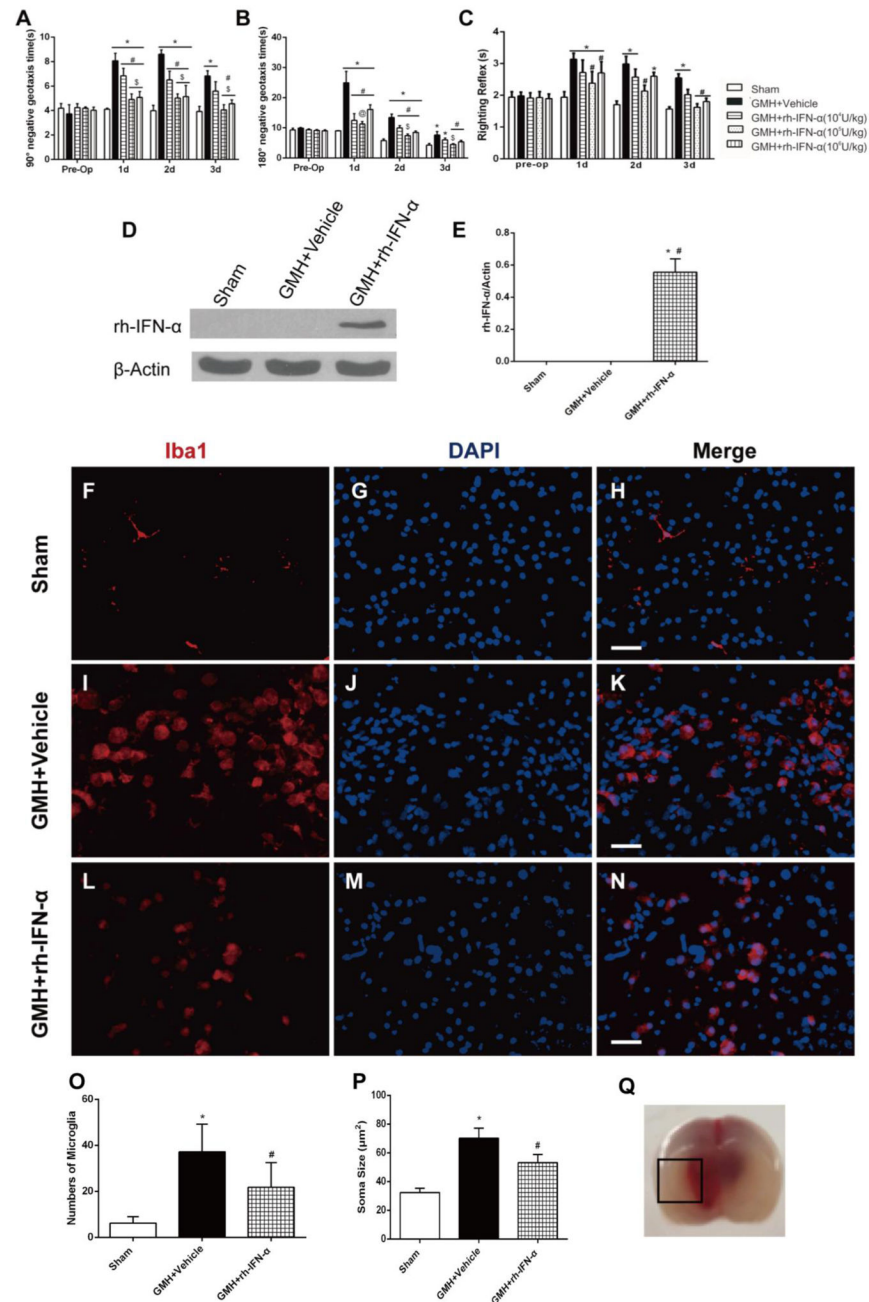
Figure 4.

Intraperitoneal administration of recombinant human interferon-α (rh-IFN-α) improved short-term neurological function 3 days after GMH and the numbers of activated microglia decreased on the 3rd day after GMH in rh-IFN-α treated animals (L, M, N and O). Negative geotaxis (A, B) and Righting reflex (C) demonstrated that medium (10^5U/kg) and high (10^6U/kg) dosage of rh-IFN-α significantly improved neurological function compared to vehicle-treated pups in the first 3 days. * P<0.001 vs Sham, # P<0.001 vs GMH + Vehicle, $ p<0.001 vs low dosage (10^4U/kg) of rh-IFN-α, @ p<0.001 vs high dosage of rh-IFN-α one-way ANOVA, Tukey's test, n=7/group. (D, E) Intraperitoneal administration of rh-IFN-α

was delivered into brain tissue at 3 days after GMH. * $P < 0.001$ vs Sham, # $P < 0.001$ vs GMH + Vehicle, one-way ANOVA, Tukey's test, n=6. Scale bar=50μm.
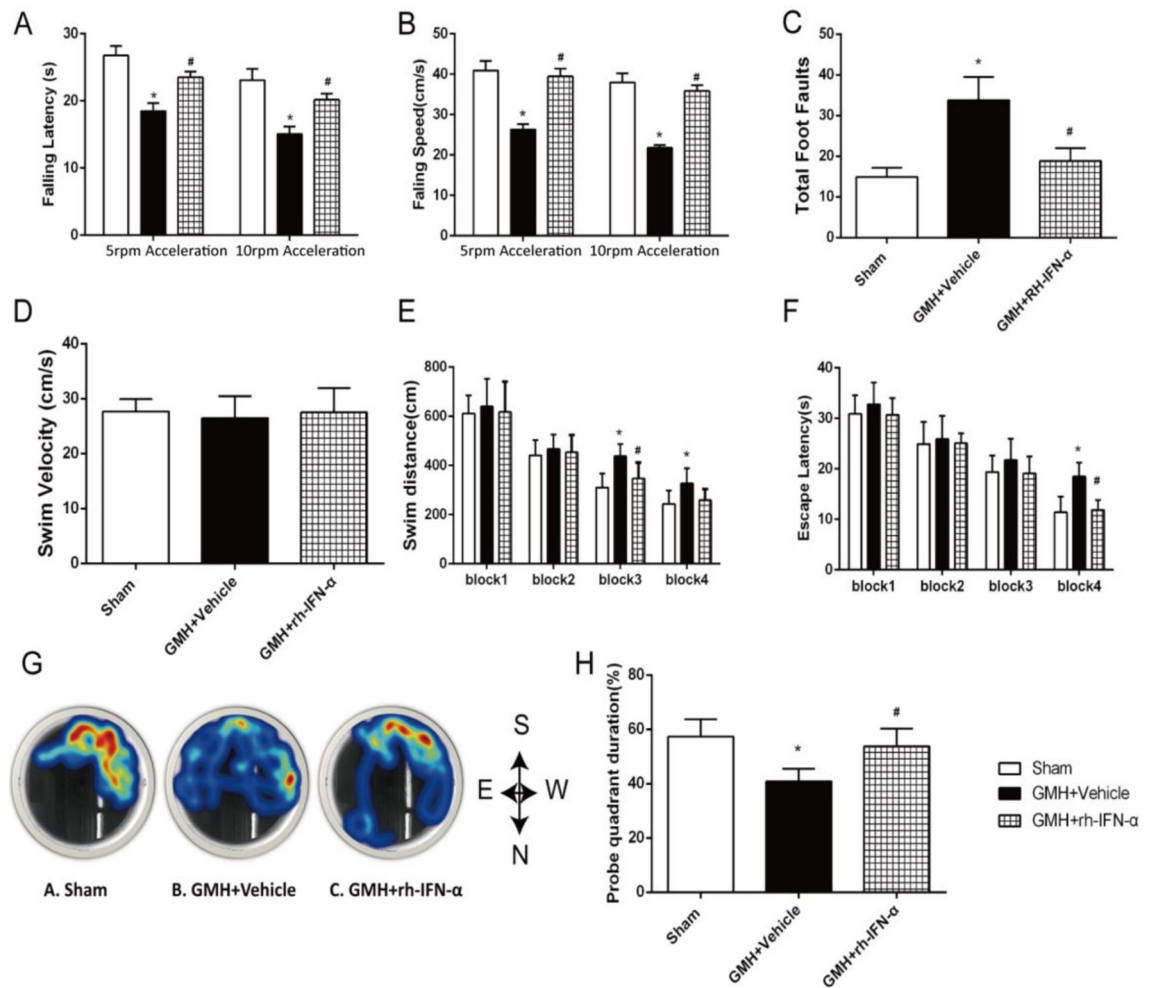
Figure 5.
rh-IFN-α administration improved long-term motor and memory function at 21-28 days after GMH. rh-IFN-α improved GMH pups' motor function evaluated by rotarod test (A, B) and foot fault (C). rh-IFN-α treatment significantly improved memory function as shown by less swim distance (E), escape latency (F) and more time in the target quadrant (G, H) in Morris water maze test, but the swim velocity (D) showed no significantly difference among three groups. * P<0.001 vs Sham, # P<0.001 vs Vehicle, one-way ANOVA, Tukey's test, n=12.
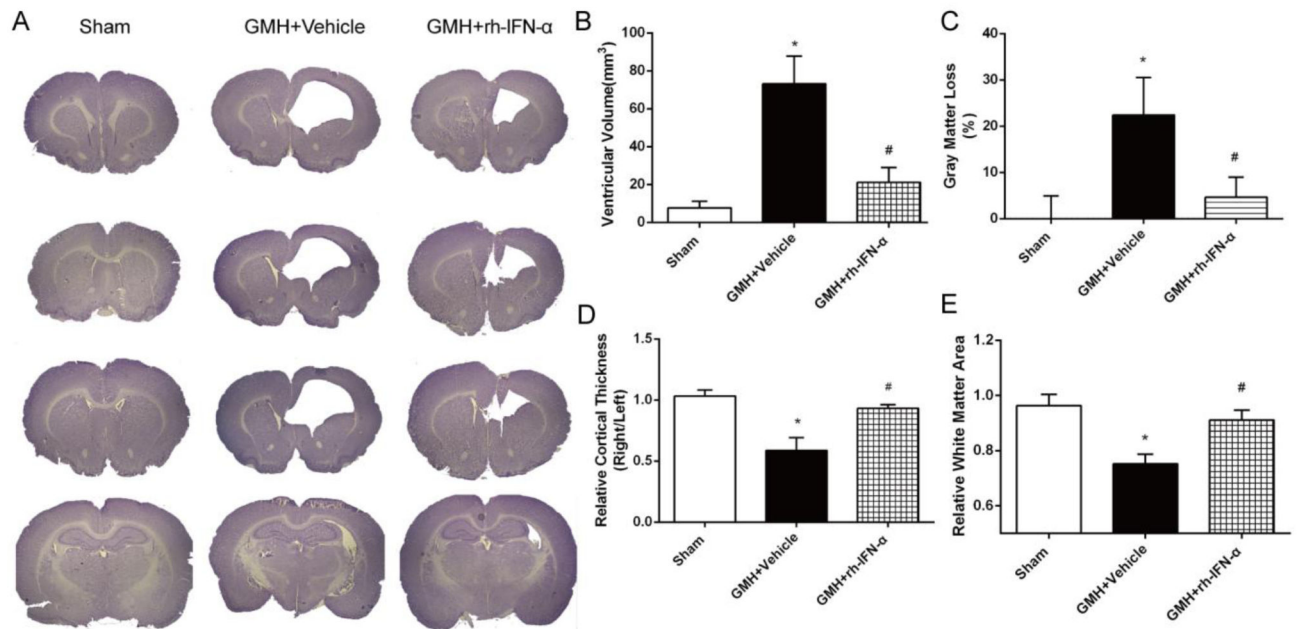
Figure 6.
rh-IFN-α administration reduced ventricular volume (A, B) and gray matter loss(C), and increased relative cortical thickness(D) and relative white matter area(E) area significantly. * P<0.001 vs Sham, # P<0.001 vs vehicle, one-way ANOVA, Tukey's test, n=6.
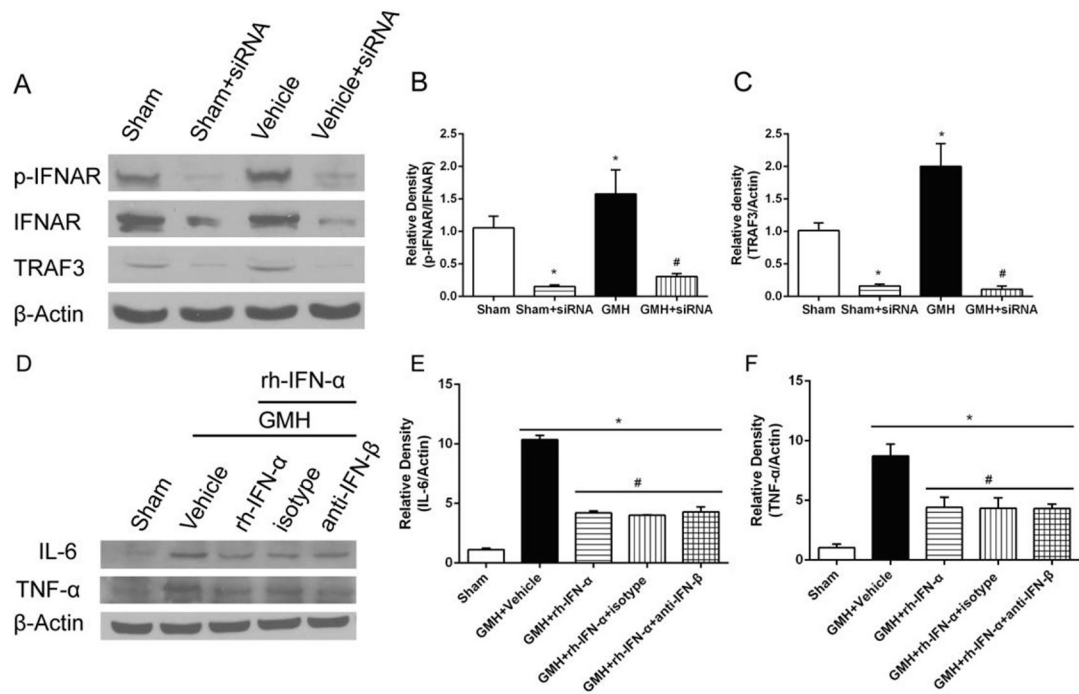
Figure 7.
Knockdown of IFNAR and TRAF3 by specific siRNA significantly inhibited the expression of IFNAR, p-IFNAR (Fig. 7A, B) and TRAF3 (Fig. 7C) in the pups 3 days after intracerebroventricular injection. The expression of inflammatory cytokines IL-6 (Fig. 7D, E) and TNF-α (Fig. 7D, F) at 3 days post GMH after neutralizing endogenous IFN-β.
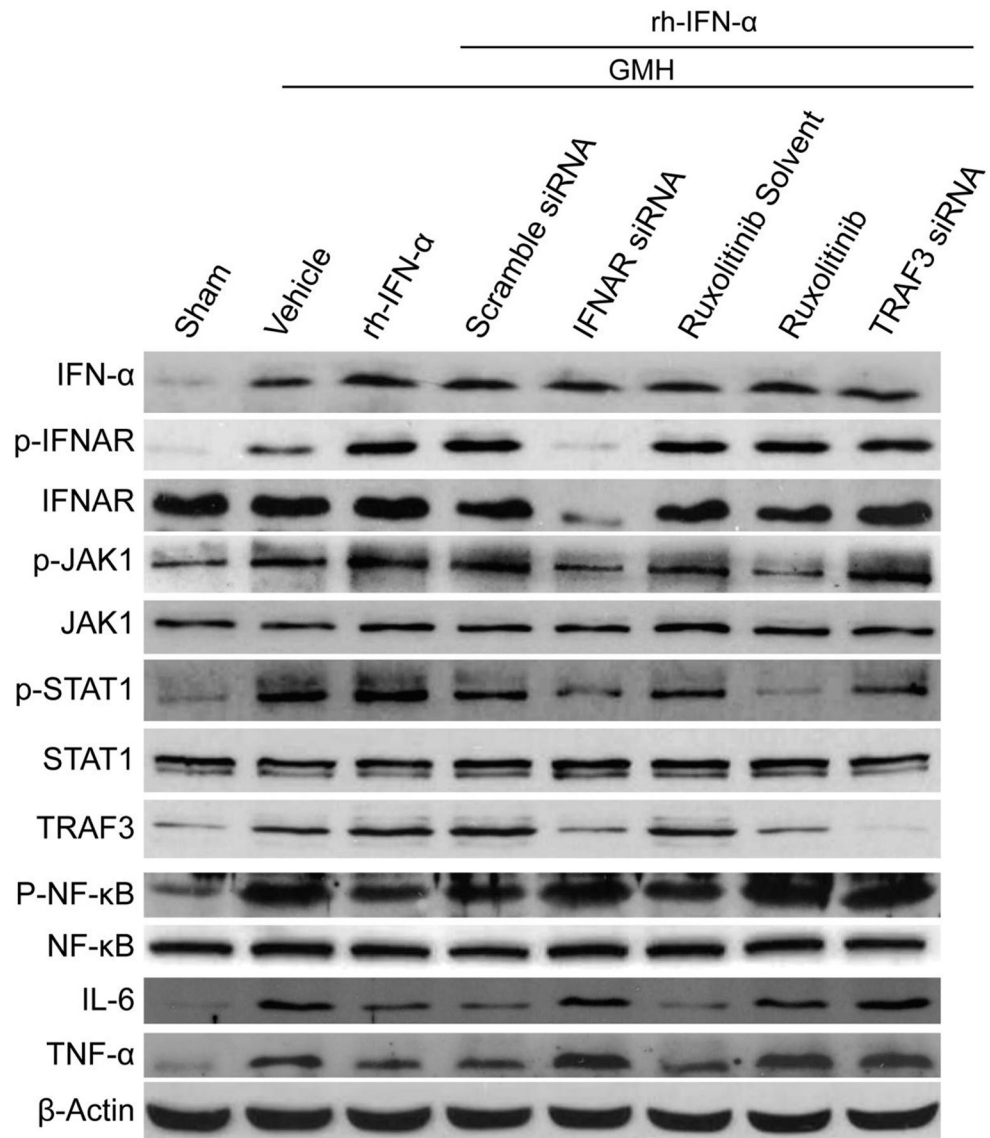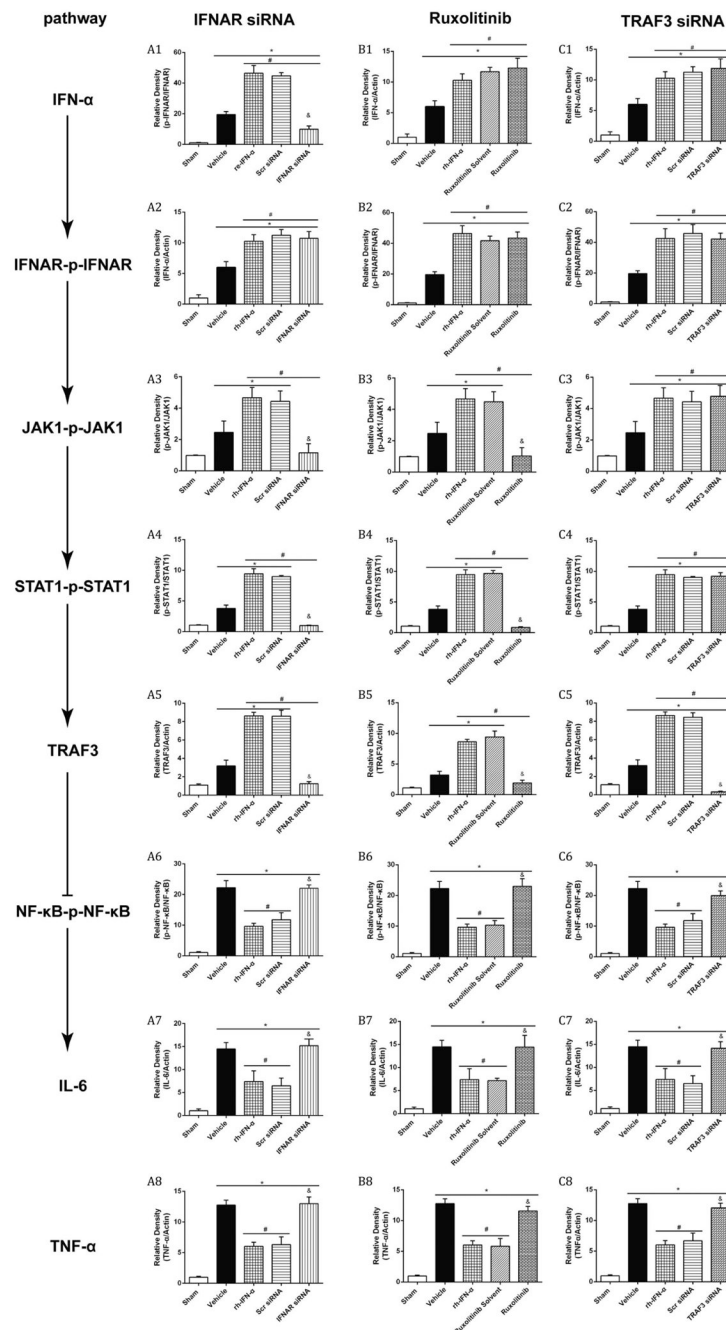
Figure 8.
Representative bands of Western blot after knockdown IFNAR, JAK1 and TRAF3
respectively.

Figure 9.
Quantitation of Western blot data of Figure 7. The expression of endogenous IFN-α
increased significantly in all treatment groups (A1, B1 and C1). IFNAR siRNA significantly
decreased p-IFNAR, IFNAR (A2), p-JAK1 (A3), p-STAT1 (A4) and TRAF3 (A5)
expression, which was accompanied by an increase of p-NF-κB (A6), IL-6 (A7) and TNF-α
(A8) 3 days after GMH. p-JAK1 (B3) was declined significantly by ruxolitinib 3 days after
intraperitoneal injection, and the expression of p-STAT1 (B4) and TRAF3 (B5) decreased
subsequently. However, p-NF-κB (B6), IL-6 (B7) and TNF-α (B8) increased significantly 3
days after GMH. The expression level of TRAF3 was significantly inhibited by its siRNA 3

days after intracerebroventricular injection, and p-NF-κB (C6), IL-6 (C7) and TNF-α (C8) maintained at high expression levels after declining of TRAF3 3 days after GMH.